Int. J. Electrochem. Sci., 17 **(2022)** Article Number: 220966, doi: 10.20964/2022.09.68

International Journal of
ELECTROCHEMICAL
SCIENCE
www.electrochemsci.org

Constructing Dual Z-scheme WO_3/Cu-g-C_3N_4/AgBr Composite Photocatalyst with Enhanced Photocatalytic Performance under Visible Light Irradiation

Jiajia Chen[1], *Haotian Liu*[1], *Yi Liu*[1,*], *Jian Yuan*[1,2], *Haibin Li*[1], *Shulong Liu*[1] *and Qiang Li*[1,*]

[1] Anhui Province Key Laboratory of Pollutant Sensitive Materials and Environmental Remediation, Huaibei Normal University, Huaibei, Anhui, 235000, P. R. China.
[2] State Key Laboratory of Applied Optics, Changchun Institute of Optics Fine Mechanics and Physics, Chinese Academy of Sciences, Changchun, 130033, P. R. China.
[*]E-mail: yiliu@chnu.edu.cn, qiangli@chnu.edu.cn

Received: 4 June 2022 / *Accepted:* 22 July 2022 / *Published:* 7 August 2022

In this work, the dual Z-scheme photocatalyst WO_3/Cu-g-C_3N_4/AgBr (WCCNB) was constructed, which shows enhanced photoactivity for decomposing MO. The results of PL and electrochemical measurements suggest that the WCCNB displays low recombination and fast transfer probability of photogenerated carriers. The improved charge separation results in a significant improvement in the photocatalytic performance. Additionally, combining with trapping experiments and band potentials of Cu-g-C_3N_4, WO_3 and AgBr, the dual Z-scheme electron migration was proposed for the WCCNB composite.

Keywords: Dual Z-scheme; g-C_3N_4; WO_3; AgBr

1. INTRODUCTION

Recently, semiconductor photocatalysis has received significant attention from researchers for solving energy and environmental crises [1, 2]. TiO_2 is a famous photocatalytic material for decomposing organic pollutants and water splitting. However, the industrial applications of TiO_2 are limited. One of its important drawbacks is the large bandgap (3.2 eV), which leads to the lack of performance in the visible spectrum [3]. For this reason, continued efforts are being made to develop visible-light-responsive photocatalysts.

Wang et al. first reported that graphitic carbon nitride (g-C_3N_4) exhibits the ability to split water for H_2 evolution in 2009 [4]. Since then, g-C_3N_4 has been researched widely as a promising visible-light-driven photocatalyst for H_2 generation, organic pollutants degradation and CO_2 reduction [5-10].

However, there are some shortcomings for g-C_3N_4 to constrain its practical application, such as inadequate light absorption and high photo-generated charge carriers recombination. Until now, tremendous efforts have been devoted to overcoming these drawbacks. Metal (such as K, Fe, Cu, Co, W, Mo and Zr) and non-metal (such as O, S, N, P and I) doping is an easy and effective strategy to change the electronic band structure and decrease the bandgap of g-C_3N_4 [11-13]. For example, Tian et al. prepared mesoporous N-doped g-C_3N_4 with improved photoabsorption properties and excellent activity for higher H_2 evolution [14]. The formation of midgap states induced by N doping could shorten the excitation path of electrons and reduce the bandgap of the g-C_3N_4, which contributes to the enhanced performance. Hu et al. found that the potentials of valence band (VB) and conduction band (CB) of g-C_3N_4 could be changed by adjusting the doping concentration of K element [15]. It was found that hydroxyl radical (•OH) and superoxide radical (•O^{2-}) could be simultaneously generated, which significantly contribute to enhancing the photodegradation of rhodamine B (RhB) under visible light irradiation. Tonda et al. reported that the electronic and optical properties of g-C_3N_4 could be markedly influenced by doping Fe [16]. The results suggested that Fe^{3+} doping could result in strongly enhanced visible light absorption and narrowed bandgap, which lead to excellent photodegradation of RhB under sunlight. Recently, Qi et al. synthesized Cu-doped g-C_3N_4 (Cu-g-C_3N_4, CCN) with surface N defects by a one-step in-situ vapor diffusion route [17]. An optimum compromise between charge carrier dynamics and improved light absorption was achieved in the as-synthesized CCN. The synergistic effects of the doped Cu and the N defects improved the activity of CCN for H_2 evolution under visible and full light spectrum irradiation.

It is widely accepted that Z-scheme heterojunction can efficiently promote the separation of the photo-induced carriers and suppress their recombination, possess powerful redox ability, and thus enhances photocatalytic activity [18-20]. Up to now, a number of g-C_3N_4-based Z-scheme heterojunctions have been constructed to improve the photoactivity of g-C_3N_4 [21-37]. Additionally, the g-C_3N_4-based Z-scheme heterojunctions were coupled with graphene oxide (GO), noble metal, and other semiconductors to promote charge separation/migration. Xu et al. found that the charge separation of Ag_2CrO_4/g-C_3N_4 composite was promoted by introducing GO nanosheets which also provide abundant photocatalytic active sites [38]. The prepared Ag_2CrO_4/g-C_3N_4/GO sample shows enhanced CO_2-conversion activity, which was ca. 2.3-fold and 1.3-fold higher than that of pristine g-C_3N_4 and Ag_2CrO_4/g-C_3N_4 heterojunction, respectively. Hu et al. synthesized ternary TiO_2/g-C_3N_4/RGO heterojunction by electrospinning technique, showing excellent RhB degradation performance [39]. It was found that the RGO network facilitated electron transfer, and the lifetime and mobility of electron were improved remarkably. Ye et al. successfully prepared Ag/Bi_4O_7/g-C_3N_4 photocatalyst, which shows enhanced visible-light photoactivity for Cr(VI) reduction [40]. In addition to the surface plasmon resonance of Ag, it was suggested that the charge separation was improved by the migration of photogenerated electrons from g-C_3N_4 to Ag. Zhu et al. synthesized non-noble-metal ternary CeO_2/MoS_2/g-C_3N_4 composite with excellent photoactivity for H_2 evolution [41]. In addition to the Z-scheme electron migration of MoS_2/g-C_3N_4 heterojunction, the transformation of electron in the CB of g-C_3N_4 to the lower CB of CeO_2 also exists. Such multi-step electron transfer behavior can efficiently promote the separation of the photoinduced carrier and enhance the performance of CeO_2/MoS_2/g-C_3N_4 composite.

WO_3 has been widely studied for the oxidation of water and photodecomposition of organic compounds under visible light. Since the band structure matches very well with g-C_3N_4, WO_3 was selected to couple with g-C_3N_4 to fabricate Z-scheme WO_3/g-C_3N_4 heterostructures in the literature, which usually exhibit excellent performance [42-44]. Furthermore, the photoactivity of Z-scheme WO_3/g-C_3N_4 can be further enhanced by introducing cocatalysts [45-51]. For example, Jiang et al. prepared a dual Z-scheme WO_3/g-C_3N_4/Bi_2O_3 photocatalyst via one step co-calcination route [46]. The reaction kinetics of the WO_3/g-C_3N_4/Bi_2O_3 sample for photodegradation of tetracycline hydrochloride was ca. 2.16-fold higher than that of WO_3/g-C_3N_4. Beyhaqi et al. reported that g-C_3N_4/WO_3/MoS_2 ternary photocatalyst shows higher degradation ability towards organic pollutants compared with g-C_3N_4/WO_3 sample [47]. Liu et al. reported a highly efficient Pt-loaded g-C_3N_4/WO_3, which has an excellent activity for photocatalytic H_2 evolution [48]. Considering that CCN exhibit shows enhanced broadened absorption, it is thus expected that WO_3/CCN (WCCN) would absorb a larger portion of solar light and exhibit better photocatalytic performance compared with WO_3/g-C_3N_4. Furthermore, we combine WCCN heterojunction with AgBr cocatalyst to construct a dual Z-scheme photocatalyst WO_3/Cu-g-C_3N_4/AgBr (WCCNB), which shows high activity for decomposing organic compounds under visible light irradiation. The as-constructed ternary WCCNB composite was carefully characterized to understand the mechanism of the enhanced performance.

2. EXPERIMENTAL SECTIONS

The synthetic route of WCCNB composite is illustrated in Scheme 1.

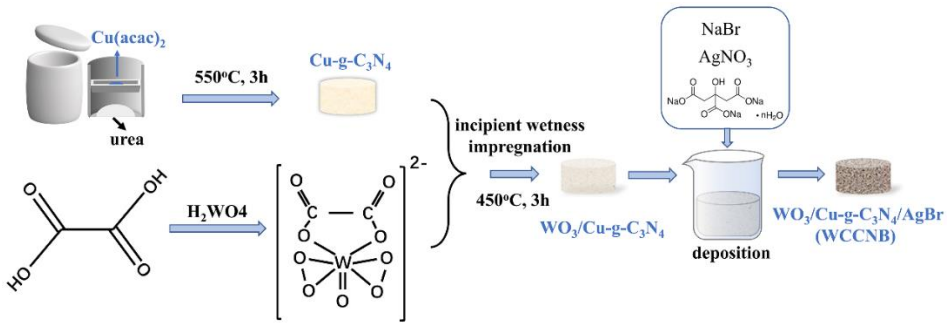

Scheme 1. The synthetic route of WCCNB composite.

The CCN was fabricated according to the previous report [17] and then added to the precursor solution of WO_3. The products obtained by the incipient wetness impregnation method were calcined in air to form WCCN heterojunctions, which were subsequently decorated with AgBr nanoparticles. Cu-g-C_3N_4/AgBr (CCNB), WO_3 and AgBr were also prepared.

2.1 Synthesis of photocatalysts

Urea (CH_4N_2O, 99.5%), tungstic acid (H_2WO_4), oxalic acid ($C_2H_2O_4{\cdot}2H_2O$, 99.5%), silver nitrate ($AgNO_3$, 99.8%), sodium citrate ($Na_3C_6H_5O_7{\cdot}2H_2O$, 99.5%), sodium bromide (NaBr, 99.0%),

ammonium oxalate ($C_2H_8N_2O_4 \cdot H_2O$, 99.5%), isopropanol (C_3H_8O, 99.7%) and p-benzoquinone ($C_6H_4O_2$, 98.0%) were purchased from Sinopharm Chemical Reagent Co., Ltd. (China).

The CCN sample was prepared according to a previously reported route. Typically, a quartz boat containing 15 mg $Cu(acac)_2$ was hung in a crucible containing 15 g urea. Subsequently, the crucible was covered and heated in a muffle furnace at 550 °C for 4 h with a ramp rate of 5 °C/min. After natural cooling to room temperature, a light-yellow CCN sample was obtained.

The WCCN sample was fabricated by an incipient wetness impregnation route. Typically, 0.05 g tungstic acid and 0.5 g oxalic acid were dissolved in 25 ml of deionized water. 1 ml of H_2O_2 was then dropped into the solution. After stirring for 3 h at 80 °C, 0.5 g CCN was added. After being ultrasonicated for 30 min and stirred for another 1 h, the mixture was heated at 100 °C for complete water evaporation. The resulting powders were calcined at 450 °C for 3 h to obtain the WCCN sample.

0.3 g of WCCN composites was ultrasonically dispersed in 50 mL of deionized water. Then, 10 mL of $AgNO_3$ solution and 10 mL of sodium citrate ($Na_3C_6H_5O_7$) solution were added and stirred for 1 h. Subsequently, 10 mL of NaBr solution was dropped into the mixture and stirred for 8 h under dark conditions. The mole ratio of $AgNO_3$, $Na_3C_6H_5O_7$ and NaBr is 1 : 0.25 : 1.1. The resulting WCCNB composites were collected by centrifuge and washed with deionized water. Finally, the WCCNB samples were dried at 70 °C for 6 h, in which the weight ratio of WCCN and AgBr is 100 : 1.

2.2 Characterization of the as-prepared samples

X-ray diffraction (XRD) data were collected using Bruker D8 Advance powder X-ray diffractometer with Cu Kα radiation. The morphology of WCCNB was characterized by field emission scanning electron microscopy (HRTEM, FEI Talos F200s). The chemical compositions and states of WCCNB were analyzed by X-ray photoelectron spectroscopy (XPS, KRATOS AXIS SUPRA+). The samples' UV-vis diffuse reflectance spectra (DRS) were acquired using $BaSO_4$ as reference material by a PerkinElmer Lambda 950 UV-vis spectrophotometer. Steady-state and time-resolved photoluminescence spectra (PL) were recorded on FLS 920 fluorescence spectrometer.

2.3 Photoelectrochemical measurements

The Photoelectrochemical measurements of as-synthesized samples were performed on a Zahner PP211 electrochemical workstation in a three-electrode cell, using a Pt plate as the counter electrode and Ag/AgCl (saturated KCl) electrode as the reference electrode. The as-prepared samples were dispersed in 1 mL of the mixed solvent containing 900 μL of ethanol and 100 μL of 5 wt% Nafion solution to form a homogeneous suspension. Then 50 μL of the suspension was coated onto FTO glass to prepare the working electrode. All photoelectrochemical experiments were carried out in 0.1 M Na_2SO_4 solution and LED irradiation (λ = 420nm).

2.4 Photocatalytic test

The photocatalytic activity of the samples was evaluated by photo-decomposing MO. The obtained photocatalysts (50 mg) were dispersed into 100 mL MO aqueous solution (15 mg L^{-1}) and stirred in a dark condition for 30 min to ensure an adsorption-desorption equilibrium before irradiation. A LED lamp (30 W, 420 nm) was the visible light source. During the photodegradation experiment, the

suspension was under continuous magnetic stirring. 3 ml of the reaction solution was taken at 3 min intervals for analysis. The MO concentration was determined at about 464 nm by UV–vis spectrophotometer. The kinetics for the degradation of MO were calculated by the pseudo-first-order equation:

$$\ln C/C_0 = -k \times t$$

where C_0 and C are the concentration of MO solution after adsorption and at the irradiation time t, respectively, k is the apparent reaction rate constant.

3. RESULTS AND DISCUSSION

Fig. 1 displays the XRD patterns of the CCN, WCCN, CCNB, WCCNB, WO_3 and AgBr samples. For the CCN sample, two peaks at 12.8° and 27.4° are assigned to the (100) and (002) diffraction planes, respectively. For the WO_3 and AgBr powders, all the peaks match well with the monoclinic structured WO_3 (JCPDS No. 71-2141) and cubic structured AgBr (JCPDS No. 79-0149), respectively. Furthermore, a small diffraction peak at around 23° was observed in the patterns of WCCN, which came from the WO_3 phase, suggesting that the WCCN composite was successfully prepared. Additionally, the AgBr phase was detected in the CCNB and WCCNB samples, indicating that the CCNB and ternary composite WCCNB were successfully prepared.

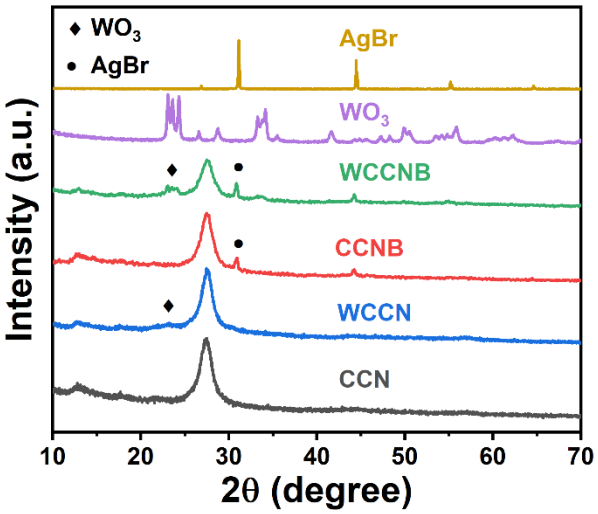

Figure 1. XRD spectra of CCN, WCCN, CCNB, WCCNB, WO_3 and AgBr powders.

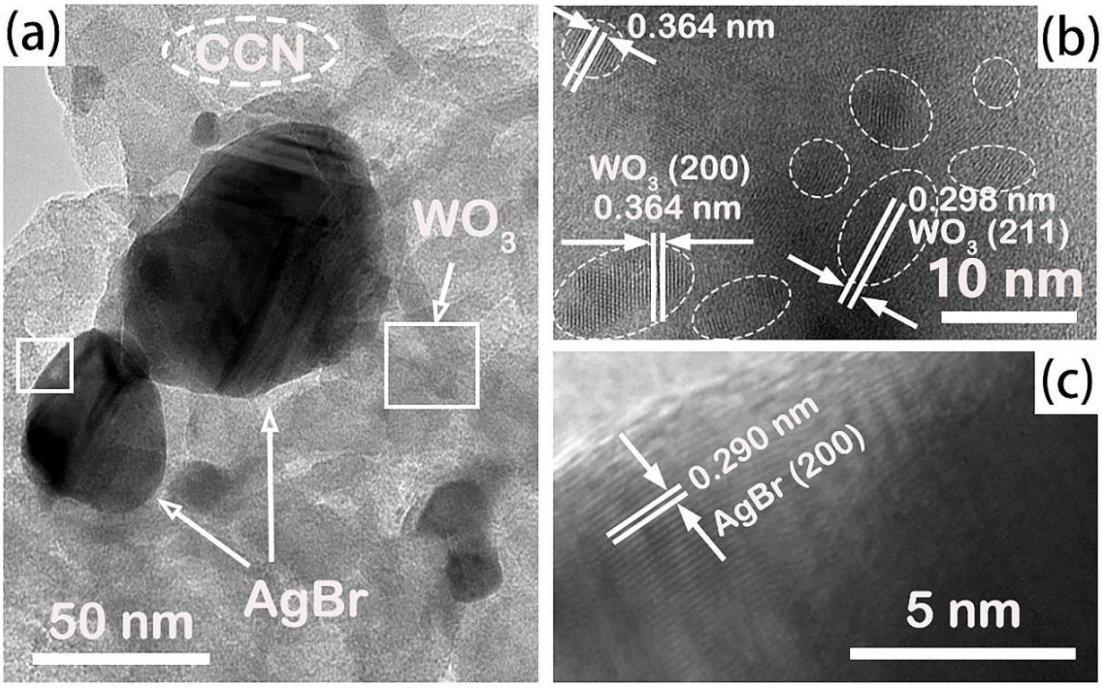

Figure 2. (a) TEM and (b, c) HRTEM images of WCCNB powder.

The microstructure of the ternary composite WCCNB was characterized by TEM (Fig. 2a). Fig. 2b and Fig. 2c exhibit the HRTEM image of marked areas in Fig. 2a. In Fig. 2b, the WO_3 crystalline grains can be observed clearly with interplanar lattice spacings of 0.364 and 0.298 nm, corresponding to (200) and (211) planes, respectively. The lattice spacing of 0.290 nm matches the (200) plane of the AgBr particles (Fig. 2c), which have a size of 50 ~ 100 nm. As indicated in the TEM and HRTEM images, the tiny WO_3 nanocrystals and AgBr nanoparticles were successfully decorated on the surface of CCN.

XPS analysis was performed to investigate the surface elements and chemical states of the WCCNB sample. As demonstrated in Fig. S1, the full spectrum of XPS reflects the existence of C, N, W, O, Ag and Br elements. Fig. 3(a-f) shows the fine XPS spectra of C 1s, N 1s, W 4f, O 1s, Ag 3d and Br 3d. From the XPS spectra of C1s (Fig. 3a), the peaks centered at 284.8, 286.5 and 288.1 eV correspond to C-C, C-N and N=C-N bonds, respectively. The N 1s band (Fig. 3b) could be divided to three peaks at around 398.6 eV, 400.4 eV and 404.4 eV, which are assigned to the C=N-C, N-$(C)_3$ bonds and π-excitation, respectively. In Fig. 3c, the XPS signal of O 1s has three peaks at 530.2, 531.8 and 533.2 eV, ascribed to O-W bond, surface OH species and adsorbed water, respectively. The existence of W^{6+} was evidenced by the W4f spectra (Fig. 3d), which could be fitted by two peaks at 37.6 and 35.4 eV, which correspond to W^{6+} $4f_{5/2}$ and $4f_{7/2}$, respectively. It indicates that WO_3 existed in the sample. Moreover, a small peak was found at 41.1 eV, which is attributed to the WO_3 loss feature. The presence of AgBr can be confirmed by the XPS spectra of Ag 3d and Br 3d. Fig. 3e shows two peaks at around 367.7 and 373.7 eV, which can be assigned to Ag^+ $3d_{3/2}$ and Ag^+ $3d_{1/2}$, respectively. The Br 3d spectrum (Fig. 3e) could be divided to two peaks at 67.8 and 68.9 eV, which are assigned to the Br^+ $3d_{3/2}$ and Br^+ $3d_{1/2}$, respectively. Additionally, since the content of Cu was too low to be detected, XPS signal of Cu was not

found, which is consistent with the reported results [17]. Based on XPS analysis, HRTEM images and XRD results, it was believed that the ternary composite WCCNS was successfully synthesized.

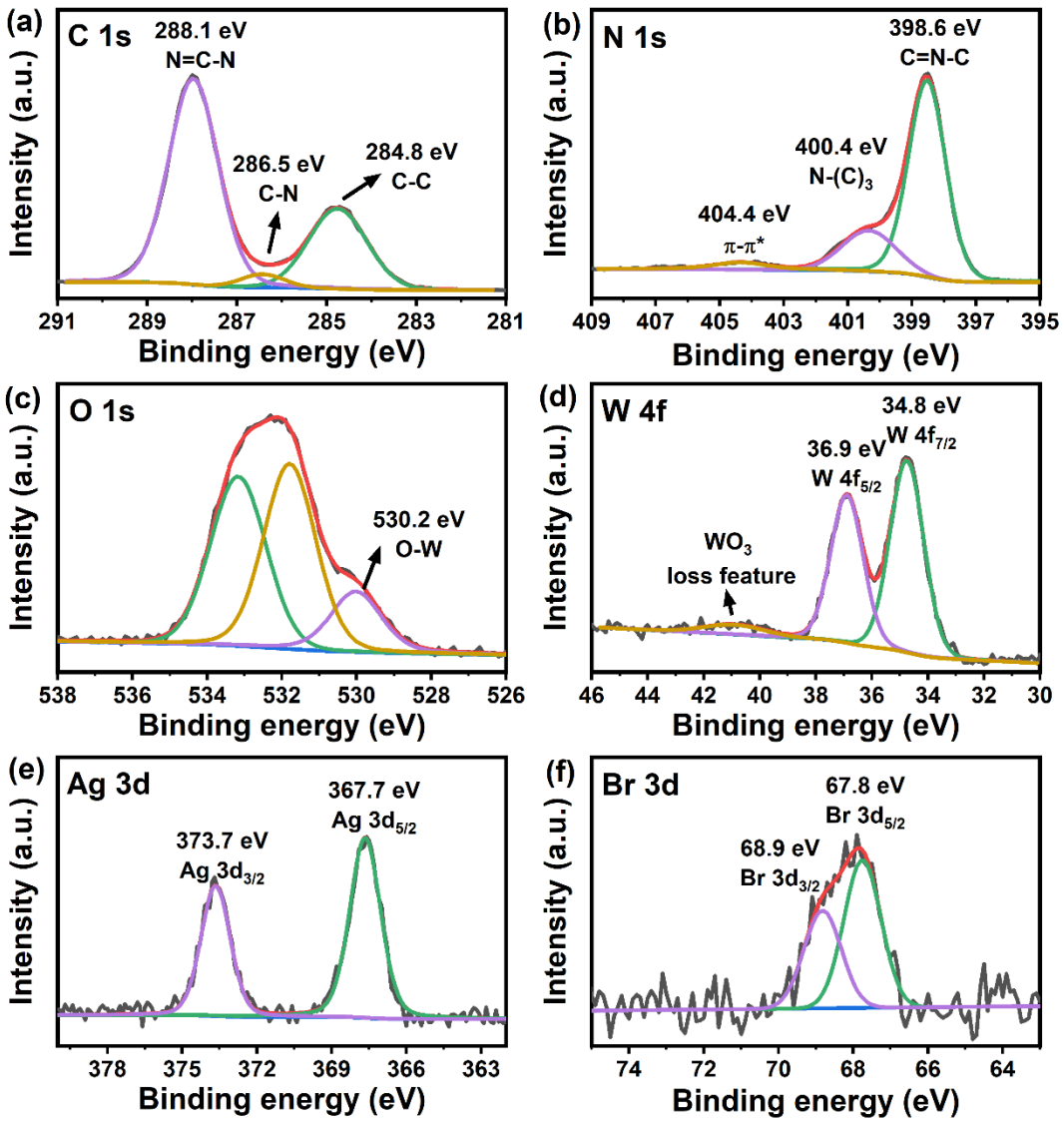

Figure 3. XPS spectra of WCCNB composite: (a) C 1s, (b) V 1s, (c) O 1s, (d) W 4f, (e) Ag 3d and (f) Br 3d.

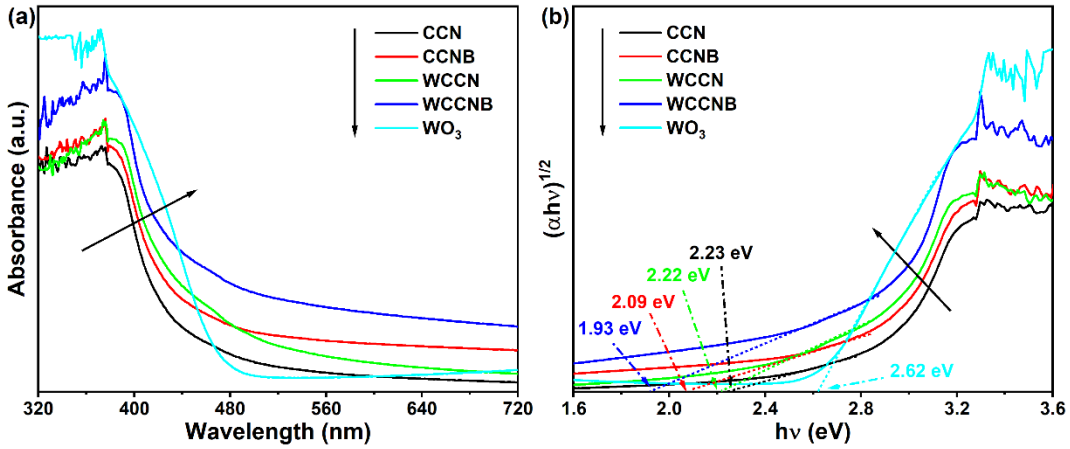

Figure 4. (a) UV-vis absorption and (b) Tauc plots of CCN, WCCN, CCNB, WCCNB, and WO_3 powders.

The optical property of the as-synthesized photocatalysts is shown in Fig. 4a. All the as-prepared CCN-based powders have light absorption capability in the visible (400 – 580 nm) range, suggesting that they are visible-active photocatalysts. The WCCNB sample exhibited a noticeable red shift of the absorption edge and enhanced light absorbance compared with other CCN-based samples, implying that it can absorb more photons. The bandgap (E_g) of the as-synthesized photocatalysts was calculated by Tauc's relation [52, 53]:

$$(\alpha h\nu)^{1/2} = A(h\nu - E_g)$$

where a, $h\nu$ and A are the absorption coefficient, the photon energy impinging on the material and a constant, respectively. Based on the Tauc plots (Fig. 4b), the bandgaps of CCN, WCCN, CCNB, WCCNB and WO_3 are estimated to be 2.23, 2.22, 2.09, 1.93 and 2.62 eV, respectively. The results indicate that the bandgap of CCN can be significantly reduced by simultaneously coupling with AgBr and WO_3.

To study the photogenerated carriers recombination in the samples, photoluminescence (PL) spectra were carried out and shown in Fig. 5a. A peak between 400 and 600 nm was observed for all samples, which may come from the radiative recombination of the photoinduced carriers in CCN. Compared to the CCN sample, the PL intensity of WCCN and CCNB decreased greatly, suggesting that the carrier recombination was reduced by combining CCN with WO_3 and AgBr, respectively. It was found that the radiative recombination was quenched in the WCCNB sample, which has the lowest PL peak, indicating that it exhibits the lowest electron-hole recombination rate. The charge transfer efficiencies in the photocatalysts were studied by time-resolved PL measurement. The recorded PL decay curve (Fig. 5b) can be fitted by a biexponential function $I(t) = f_1 \exp(-t/\tau_1) + f_2 \exp(-t/\tau_2)$ [48]. The fitting results are listed in Table 1.

Table 1. Fitted parameters from time-resolved PL curve of CCN, WCCN, CCNB and WCCNB powders.

Sample	τ_1 (ns)	τ_2 (ns)	f_1	f_2	τ_{avg} (ns)[a]
CN	2.48	10.3	802.57	229.13	6.72
CCNB	2.309	9.60	773.05	223.60	6.29
WCCN	2.29	8.90	876.08	192.91	5.34
WCCNB	1.92	8.02	835.24	187.96	4.88

[a]The average charger lifetime (τ_{avg}) was calculated according to the equation:

$$\tau_{avg} = (f_1 \tau_1^2 + f_2 \tau_2^2)/(f_1 \tau_1 + f_2 \tau_2)$$

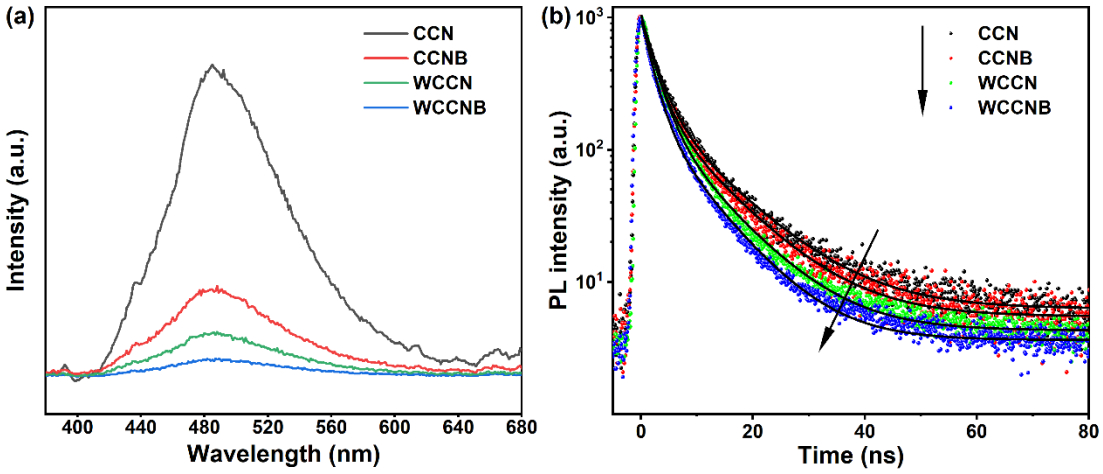

Figure 5. (a) PL and (b) time-resolved PL decay spectra spectrum of CCN, WCCN, CCNB and WCCNB powders.

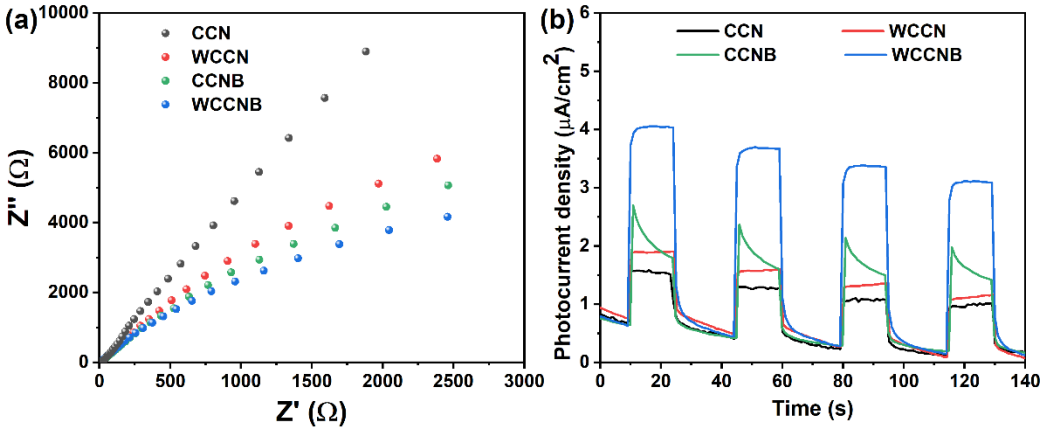

Figure 6. (a) EIS Nyquist plots and (b) photocurrent responses of CCN, WCCN, CCNB and WCCNB.

It is found that the average charger lifetime (τ_{avg}) of the as-prepared CCN-based samples decreases in the order of CCN > CCNB > WCCN > WCCNS, and the τ_{avg} was estimated to be 6.72 ns, 6.29 ns, 5.34 ns and 4.88 ns, respectively. WCCNS has the lowest τ_{avg}, suggesting that it has the fastest transfer of photogenerated charge carriers.

The efficient charge transfer and separation were also confirmed by electrochemical measurements. The electrochemical impedance spectroscopy (EIS) (Fig. 6a) presents that WCCNB has the lowest resistance, which is favorable for charge transfer. According to the photocurrent responses under intermittent irradiation (Fig. 6b), it can be seen that the photocurrent density of the ternary WCCNB composite is much higher than that of other photocatalysts, indicating that the WCCNB possesses higher charge separation efficiency.

The photoactivity of the as-synthesized catalysts was evaluated by degrading methylene orange (MO) under LED light irradiation (λ = 420 nm), as shown in Fig. 7a. After 15 min of illumination, 75% of MO was degraded by CCN. When the binary catalysts were used, 80% and 90% of MO were degraded over WCCN and CCNB, respectively. It is found that the photocatalytic performance of CCN can be simply improved by coupling with WO_3 or AgBr. Compared with other photocatalysts, the ternary composite WCCNB exhibits enhanced photocatalytic activity, which successfully removes 97% of MO within 12 min. The kinetics of photocatalytic degradation of MO were found to follow pseudo-first-order model for all the photocatalysts, as displayed in Fig. 7b. The apparent reaction rate constant *k* obtained over the WCCNB photocatalyst was about 3.96, 2.76 and 1.94 times as high as that over CCN, WCCN and CCNB, respectively. The WCCNB photocatalyst exhibits excellent photocatalytic performance, which might arise from the inhibited recombination and promoted charge separation of the photogenerated carriers. The photocatalytic activity of WCCNB for pollutant degradation is superior to that of most of the reported g-C_3N_4/WO_3-based photocatalysts (Table 2).

Table 2. Comparison of photocatalytic activity for pollutant degradation over g-C_3N_4/WO_3-based materials.

Photocatalyst	Reactant solution	Light source	Photocatalytic rate *k* (min^{-1})	Ref.
WCCNB	50 mg photocatalyst, MO (100 mL, 15 mg L^{-1})	30 W LED light (420 nm)	0.25	This work
g-C_3N_4/WO_3/MoS_2	100 mg photocatalyst, RhB (100 mL, 50 ppm) 100 mg photocatalyst, MO (100 mL, 20 ppm)	300 W Xeon lamp (λ ≥ 420 nm)	0.097 0.0325	[47]
WO_3/Ag/g-C_3N_4	100 mg photocatalyst, RhB (300 mL, 10 mg L^{-1})	500 W Xeon lamp (λ ≥ 420 nm)	0.053	[54]
Ag-AgCl/WO_3/g-C_3N_4	50 mg photocatalyst, Trimethoprim (100 mL, 4 mg L^{-1})	500 W metal halogen lamp (λ ≥ 400 nm)	0.156	[50]
WO_3/g-C_3N_4/Bi_2O_3	100 mg photocatalyst, Tetracycline hydrochloride (100 mL, 10 mg L^{-1})	300 W Xeon lamp (λ ≥ 420 nm)	0.023	[46]
g-C_3N_4/WO_3	50 mg photocatalyst, Methylparaben (50 mL, 15 mg L^{-1})	300 W Xeon lamp (with an IR cut filter)	0.0795	[55]

To understand the main active species in the photodegradation of MO over WCCNB, ammonium oxalate (AO), p-benzoquinone (BQ) and isopropanol (IPA) were employed for trapping h^+, $^{\bullet}OH$ and $^{\bullet}O_2^-$, respectively [56, 57]. As displayed in Fig. 7c, when IPA was added, a slight decrease in the photocatalytic performance of WCCNB was observed. On the contrary, when h^+ and $^{\bullet}OH$ were trapped by adding AO and BQ, the photocatalytic ability for the degradation of MO decreased considerably. The results of trapping experiments suggested that the photocatalytic decomposition of MO was driven mainly by the participation of h^+ and $^{\bullet}OH$ and lesser extent by the participation of $^{\bullet}O_2^-$. Additionally, the recycled experiments were carried out to study the photocatalytic stability of WCNNB. No decrease in catalytic activity is observed in the recycling reactions (Fig. 7d), demonstrating that the synthesized ternary WCCNS photocatalyst possesses good recyclability.

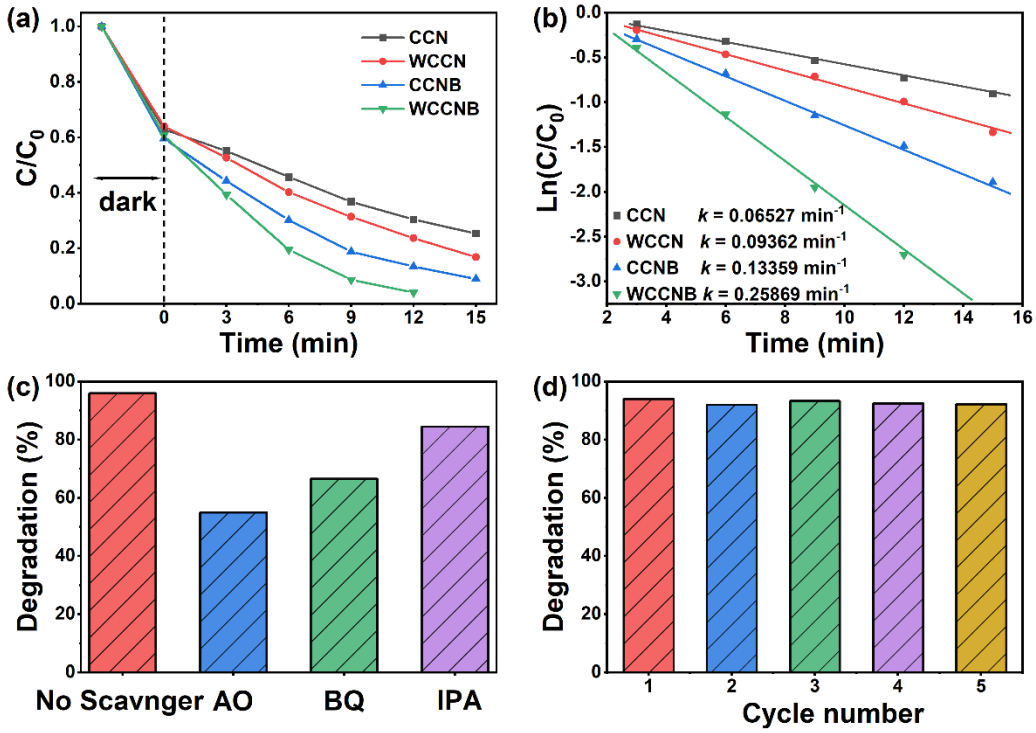

Figure 7. (a) Photocatalytic degradation of MO over the CCN, WCCN, CCNB and WCCNB powders; (b) Kinetic curves of MO photodegradation over the CCN, WCCN, CCNB and WCCNB powders; (c) The reusability of the WCCNB photocatalyst; (d) Photodegradation efficiency of MO over the WCCNB photocatalyst in the presence of AO, BQ and IPA.

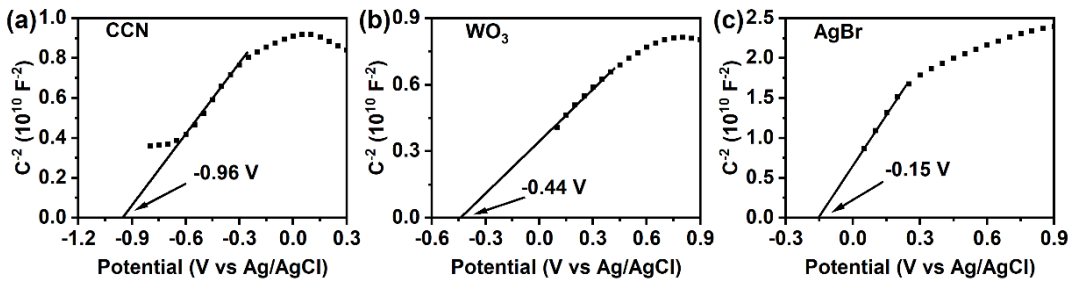

Figure 8. Mott-Schottky plots of the CCN, WO_3 and AgBr.

In Fig. 8, the positive slope of the Mott-Schottky plots demonstrated that CCN, WO_3 and AgBr are n-type semiconductors, and their flat band potential (E_{fb}) are estimated to be -0.96, -0.44 and -0.15 V vs. Ag/AgCl electrode, respectively. For most n-type semiconductors, it was generally believed that conduction band (CB) edge potential (E_{CB}) is slightly smaller than E_{fb} (~ 0.1 eV) [58, 59]. The E_{CB} and valence band (VB) edge position (E_{VB}) can be calculated by the following equations:

$$E_{CB} = E_{fb} + 0.198 - 0.1$$

$$E_{VB} = E_{CB} - E_g$$

Fig. S2 demonstrated that the E_g of the as-prepared AgBr is 2.51 eV. Therefore, for the CCN, WO_3 and AgBr, the E_{CB} are -0.86, -0.34 and -0.05 V vs. NHE, respectively, and E_{VB} are +1.37, +2.28 and +2.46 V vs. NHE, respectively.

Based on the band potentials of CCN, WO_3 and AgBr, the photodegradation mechanism of the ternary WCCNB photocatalyst was illustrated in Fig. 9. Under LED light irradiation, holes and electrons were generated in the VB and CB of CCN, WO_3 and AgBr. It should be noted that the photoexcited holes in the VB of CCN cannot be scavenged by the OH^- to yield $^{\bullet}OH$ radicals due to its higher redox potential (~ 1.37 V vs. NHE) as compared to the $^{\bullet}OH/OH^-$ potential (1.90 V vs. NHE) [60, 61]. Based on the results of the trapping experiment, it is unreasonable that photoinduced holes in the surface of WO_3 and AgBr transfer to CCN according to the type-II heterojunction (Fig. 9a).

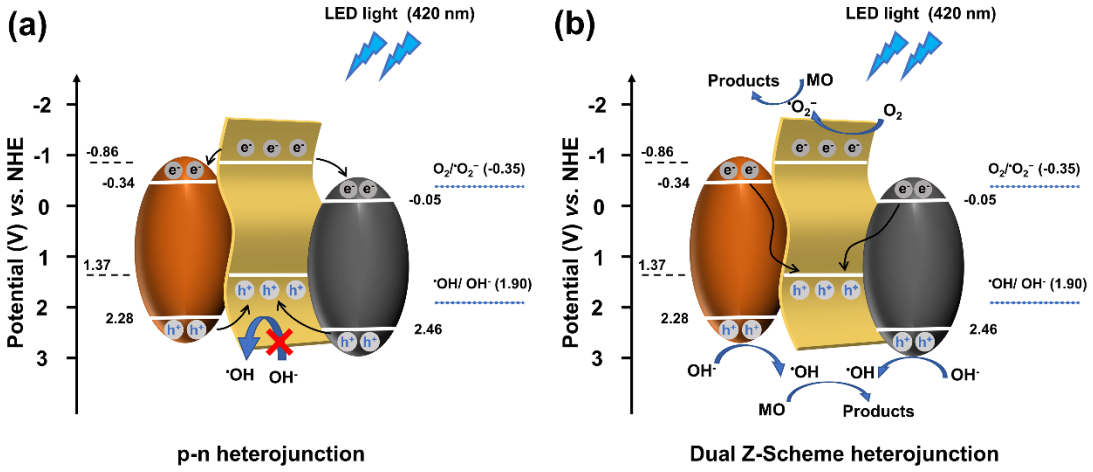

Figure 9. Schematic illustrating the photodegradation mechanism of MO over the WCCNB photocatalyst.

It is supposed that a dual Z-scheme electron transfer occurs in the WCCNB composites (Fig. 9b). The photoexcited electrons in the CB of WO_3 and AgBr would recombine with the photogenerated holes in the VB of CCN. Because the VB potentials of WO_3 and AgBr (+2.28 and +2.46 V vs. NHE) are below the $^{\bullet}OH/OH^-$ potential, the OH^- could be converted to the $^{\bullet}OH$ radicals by reacting with the photoexcited holes in the VB of WO_3 and AgBr. Simultaneously, the photoexcited electrons in the surface of CCN

could react with O_2 to create $O_2^{\bullet-}$ for MO degradation. Compared with $O_2^{\bullet-}$, the formed $^{\bullet}OH$ and holes could more effectively break down MO molecule.

4. CONCLUSIONS

The dual Z-scheme WCCNB photocatalyst was successfully fabricated, which shows enhanced photocatalytic performance under LED light. The efficient charge transfer and separation were achieved in the ternary WCCNB composite, which improved photoactivity. Based on the trapping experiment results and band positions, a double Z-scheme electron transfer path was proposed in the WCCNB photocatalyst.

SUPPORTING MATERIAL

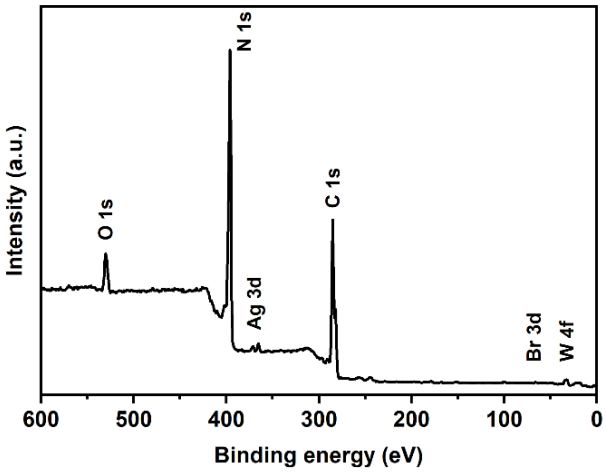

Fig. S1. XPS spectra of WCCNB

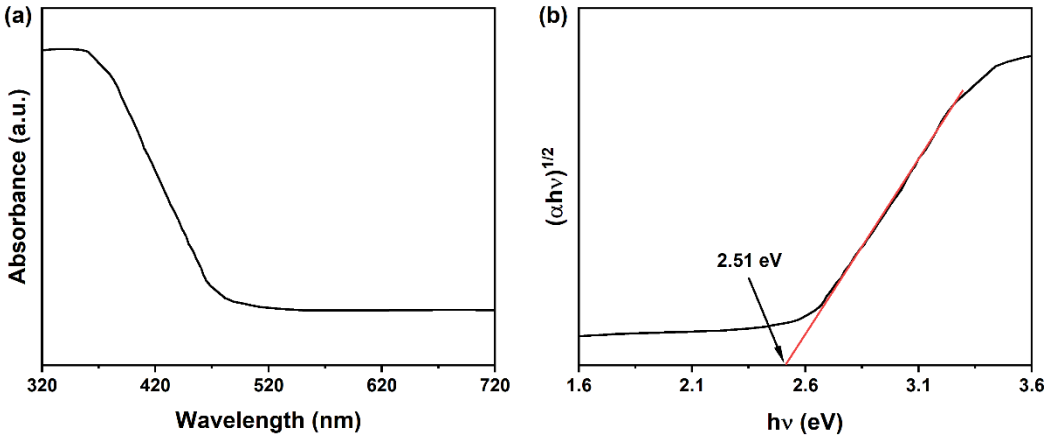

Fig. S2. (a) UV-vis absorption and (b) Tauc plots of AgBr powders.

CONFLICTS OF INTEREST
There are no conflicts to declare.

ACKNOWLEDGEMENTS
This work was supported by Anhui Provincial Natural Science Foundation (1908085QE222, 1908085QF293, 2008085QF319), the Natural Science Foundation of the Anhui Higher Education Institutions of China (KJ2020B02, KJ2020A0047, KJ2020A1194, KJ2021A0518), Quality Engineering (2020xkcsz010, 2020sxzx47), Undergraduate Innovation and Entrepreneurship Program (202110373147, 202110373014), State Key Laboratory of applied optics (SKLAO2022001A13) and the Open Project of Anhui Province Key Laboratory of Pollutant Sensitive Materials and Environmental Remediation.

References

1. F. Fresno, R. Portela, S. Suarez and J.M. Coronado, *J. Mater. Chem. A*, 2 (2014) 2863.
2. X.B. Chen, S.H. Shen, L.J. Guo and S.S. Mao, *Chem. Rev.*, 110 (2010) 6503.
3. A.L. Linsebigler, G. Lu and J.T. Yates, *Chem. Rev.*, 95 (1995) 735.
4. X.C. Wang, K. Maeda, A. Thomas, K. Takanabe, G. Xin, J.M. Carlsson, K. Domen and M. Antonietti, *Nat. Mater.*, 8 (2009) 76.
5. U. Ghosh, A. Majumdar and A. Pal, *J. Environ. Chem. Eng.*, 9 (2021) 104631.
6. C. Prasad, H. Tang, Q. Liu, I. Bahadur, S. Karlapudi and Y. Jiang, *Int. J. Hydrogen Energy*, 45 (2020) 337.
7. A. Mishra, A. Mehta, S. Basu, N.P. Shetti, K.R. Reddy and T.M. Aminabhavi, *Carbon*, 149 (2019) 693.
8. X.L. Liu, R. Ma, L. Zhuang, B.W. Hu, J.R. Chen, X.Y. Liu and X.K. Wang, *Crit. Rev. Env. Sci. Technol.*, 51 (2020) 751.
9. Z.S. Chen, S. Zhang, Y. Liu, N.S. Alharbi, S.O. Rabah, S. Wang and X.X. Wang, *Sci. Total Environ.*, 731 (2020) 139054.
10. W.J. Ong, L.L. Tan, Y.H. Ng, S.T. Yong and S.P. Chai, *Chem. Rev.*, 116 (2016) 7159.
11. S. Patnaik, D.P. Sahoo and K. Parida, *Carbon*, 172 (2021) 682.
12. L. Zhou, H.Y. Zhang, H.Q. Sun, S.M. Liu, M.O. Tade, S.B. Wang and W.Q. Jin, *Catal. Sci. Technol.*, 6 (2016) 7002.
13. M.L. Zhang, Y. Yang, X.Q. An and L. Hou, *Chem. Eng. J.*, 412 (2021) 128663.
14. N. Tian, Y. Zhang, X. Li, K. Xiao, X. Du, F. Dong, G.I.N. Waterhouse, T. Zhang and H. Huang, *Nano Energy*, 38 (2017) 72.
15. S.Z. Hu, F.Y. Li, Z.P. Fan, F. Wang, Y.F. Zhao and Z.B. Lv, *Dalton Trans.*, 44 (2015) 1084.
16. S. Tonda, S. Kumar, S. Kandula and V. Shanker, *J. Mater. Chem. A*, 2 (2014) 6772.
17. R.J. Qi, P.F. Yu, J.C. Zhang, W.Q. Guo, Y.Y. He, H. Hojo, H. Einaga, Q. Zhang, X.S. Liu, Z. Jiang and W.F. Shangguan, *Appl. Catal., B*, 274 (2020) 119099.
18. X.L. Liu, Q.Z. Zhang and D.L. Ma, *Sol. RRL*, 5 (2021) 2000397.
19. H.J. Li, W.G. Tu, Y. Zhou and Z.G. Zou, *Adv. Sci.*, 3 (2016) 1500389.
20. P. Zhou, J.G. Yu and M. Jaroniec, *Adv. Mater.*, 26 (2014) 4920.
21. J.C. Wang, H.C. Yao, Z.Y. Fan, L. Zhang, J.S. Wang, S.Q. Zang and Z.J. Li, *ACS Appl. Mater. Interfaces*, 8 (2016) 3765.
22. X.J. She, J.J. Wu, H. Xu, J. Zhong, Y. Wang, Y.H. Song, K.Q. Nie, Y. Liu, Y.C. Yang, M.-T.F. Rodrigues, R. Vajtai, J. Lou, D.L. Du, H.M. Li and P.M. Ajayan, *Adv. Energy Mater.*, 7 (2017) 1700025.
23. Q.L. Xu, B.C. Zhu, C.J. Jiang, B. Cheng and J.G. Yu, *Sol. RRL*, 2 (2018) 1800006.

24. P.F. Xia, B.C. Zhu, B. Cheng, J.G. Yu and J.S. Xu, *ACS Sustainable Chem. Eng.*, 6 (2018) 965.
25. Y.Y. Shi, M.C. Zhang, Y.M. Li, G.J. Liu, R.C. Jin, Q.Y. Wang, H. Xu and S.M. Gao, *Ceram. Int.*, 46 (2020) 25905.
26. S. Panimalar, R. Uthrakumar, E.T. Selvi, P. Gomathy, C. Inmozhi, K. Kaviyarasu and J. Kennedy, *Surf. Interfaces*, 20 (2020) 100512.
27. Y. Wang, G.Q. Tan, T. Liu, Y.N. Su, H.J. Ren, X.L. Zhang, A. Xia, L. Lv and Y. Liu, *Appl. Catal., B*, 234 (2018) 37.
28. M. Ou, S.P. Wan, Q. Zhong, S.L. Zhang, Y. Song, L.N. Guo, W. Cai and Y.L. Xu, *Appl. Catal., B*, 221 (2018) 97.
29. Y.X. Zhu, Y.J. Cui, B.B. Xiao, J. Ou-yang, H.P. Li and Z.R. Chen, *Mater. Sci. Semicond. Process.*, 129 (2021) 105767.
30. W.L. Zhao, W.L. Wang and H.F. Shi, *Appl. Surf. Sci.*, 528 (2020) 146925.
31. Z.S. Wu, X.F. He, Y.T. Xue, X. Yang, Y.F. Li, Q.B. Li and B. Yu, *Chem. Eng. J.*, 399 (2020) 125747.
32. X.Y. Gu, J. Mei, J.H. Lai, S.Y. Lv, J. Yang, S.H. Cui and S. Chen, *Mater. Res. Bull.*, 130 (2020) 110939.
33. U. Ghosh and A. Pal, *Appl. Surf. Sci.*, 507 (2020) 144965.
34. M. Alhaddad, R.M. Navarro, M.A. Hussein and R.M. Mohamed, *Ceram. Int.*, 46 (2020) 24873.
35. K.R.S. Devi, S. Mathew, R. Rajan, J. Georgekutty, K. Kasinathan, D. Pinheiro and S. Sugunan, *Appl. Surf. Sci.*, 494 (2019) 465.
36. H. Huang, Y.X. Li, H.L. Wang and W.F. Jiang, *Appl. Surf. Sci.*, 538 (2021) 148132.
37. B. Zhang, H.X. Shi, Y.J. Yan, C.Q. Liu, X.Y. Hu, E.Z. Liu and J. Fan, *Colloids Surf., A*, 608 (2021) 125598.
38. D.F. Xu, B. Cheng, W.K. Wang, C.J. Jiang and J.G. Yu, *Appl. Catal., B*, 231 (2018) 368.
39. L.M. Hu, J.T. Yan, C.L. Wang, B. Chai and J.F. Li, *Chin. J. Catal.*, 40 (2019) 458.
40. M. Ye, W. Wei, L. Zheng, Y. Liu, D. Wu, X. Gu and A. Wei, *J. Hazard. Mater.*, 365 (2019) 674.
41. C.Z. Zhu, Y.T. Wang, Z.F. Jiang, F.C. Xu, Q.M. Xian, C. Sun, Q. Tong, W.X. Zou, X.G. Duan and S.B. Wang, *Appl. Catal., B*, 259 (2019) 118072.
42. J. Ding, Q.Q. Liu, Z.Y. Zhang, X. Liu, J.Q. Zhao, S.B. Cheng, B.N. Zong and W.L. Dai, *Appl. Catal., B*, 165 (2015) 511.
43. H.Q. Zhuang, Z.P. Cai, W.T. Xu, M.L. Huang and X.B. Liu, *New J. Chem.*, 43 (2019) 17416.
44. H. Katsumata, Y. Tachi, T. Suzuki and S. Kaneco, *RSC Adv.*, 4 (2014) 21405.
45. J.Q. Li, H.J. Hao and Z.F. Zhu, *Mater. Lett.*, 168 (2016) 180.
46. L.B. Jiang, X.Z. Yuan, G.M. Zeng, J. Liang, X.H. Chen, H.B. Yu, H. Wang, Z.B. Wu, J. Zhang and T. Xiong, *Appl. Catal., B*, 227 (2018) 376.
47. A. Beyhaqi, Q.Y. Zeng, S. Chang, M.Q. Wang, S.M. Taghi Azimi and C. Hu, *Chemosphere*, 247 (2020) 125784.
48. D. Liu, S. Zhang, J.M. Wang, T.Y. Peng and R.J. Li, *ACS Appl. Mater. Interfaces*, 11 (2019) 27913.
49. S. Ali, M. Humayun, W. Pi, Y. Yuan, M. Wang, A. Khan, P. Yue, L. Shu, Z.P. Zheng, Q.Y. Fu and W. Luo, *J. Hazard. Mater.*, 397 (2020) 122708.
50. G.D. Fan, R.S. Ning, Z.S. Yan, J. Luo, B.H. Du, J.J. Zhan, L.S. Liu and J. Zhang, *J. Hazard. Mater.*, 403 (2021) 123964.
51. L.X. Liu, A.J. He and X. Yao, *Int. J. Electrochem. Sci.*, 17 (2022) 220635.
52. M.A. Butler, *J. Appl. Phys.*, 48 (1977) 1914.
53. B.D. Viezbicke, S. Patel, B.E. Davis and D.P. Birnie III, *Phys. Status Solidi B*, 252 (2015) 1700.
54. J. Chen, X. Xiao, Y. Wang and Z. Ye, *Appl. Surf. Sci.*, 467-468 (2019) 1000.
55. X. Zhang, X. Wang, J. Meng, Y. Liu, M. Ren, Y. Guo and Y. Yang, *Sep. Purif. Technol.*, 255 (2021) 117693.
56. H.B. Fu, C.S. Pan, W.Q. Yao and Y.F. Zhu, *J. Phys. Chem. B*, 109 (2005) 22432.

57. G. Sivalingam, K. Nagaveni, M.S. Hegde and G. Madras, *Appl. Catal., B*, 45 (2003) 23.
58. Y. Matsumoto, *J. Solid State Chem.*, 126 (1996) 227.
59. A. Ishikawa, T. Takata, J.N. Kondo, M. Hara, H. Kobayashi and K. Domen, *J. Am. Chem. Soc.*, 124 (2002) 13547.
60. M. Kaneko and I. Okura, *Photocatalysis: science and technology*, Springer, 2002.
61. D.A. Armstrong, R.E. Huie, W.H. Koppenol, S.V. Lymar, G. Merényi, P. Neta, B. Ruscic, D.M. Stanbury, S. Steenken and P. Wardman, *Pure Appl. Chem.*, 87 (2015) 1139.